Electronic Supplementary Material (ESI) for Nanoscale.

Supporting Information

Multi-gate Memristive Synapses Realized with Lateral Heterostructures of 2D WSe_2 and WO_3

Hui-Kai He, Rui Yang*, He-Ming Huang, Fan-Fan Yang, Ya-Zhou Wu, Jamal Shaibo, Xin Guo*

State Key Laboratory of Material Processing and Die & Mould Technology, Laboratory of Solid State Ionics, School of Materials Science and Engineering, Huazhong University of Science and Technology, Wuhan 430074, P. R. China

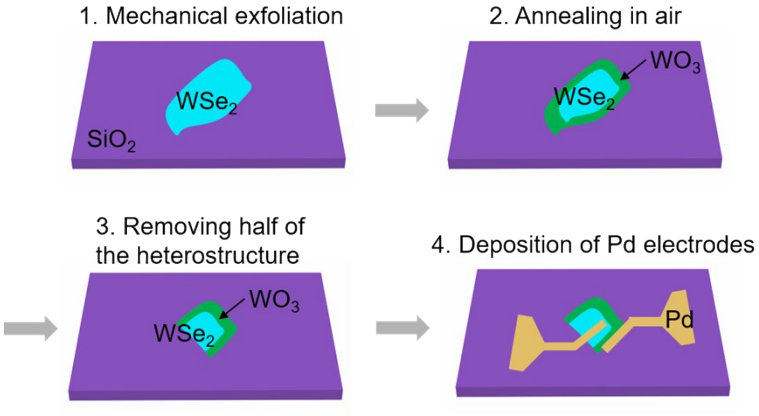

Figure S1. Fabrication process of Pd-WSe_2-WO_3-Pd memristive devices.

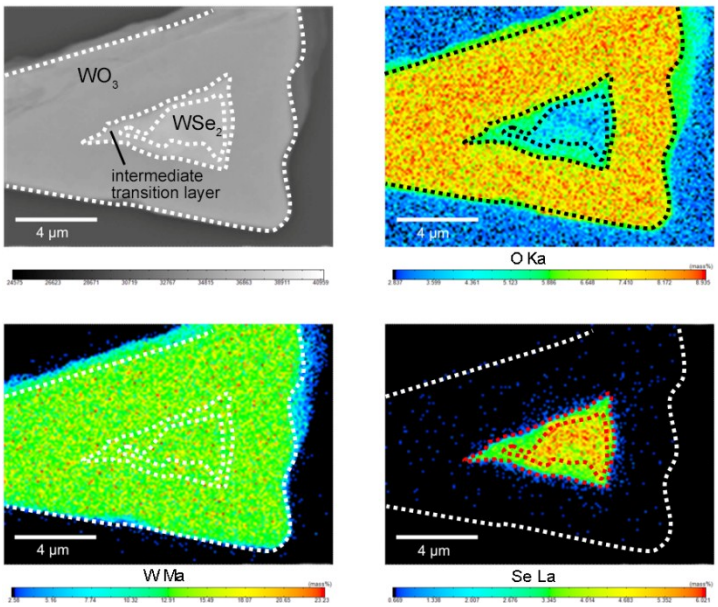

Figure S2. Electron-probe microanalyzer (EPMA) composition analysis of the WO_3-WSe_2 heterostructure. One can clearly see three regions in the heterostructure, *i.e.*, a WO_3 region, a WSe_2 region and an intermediate transition layer.

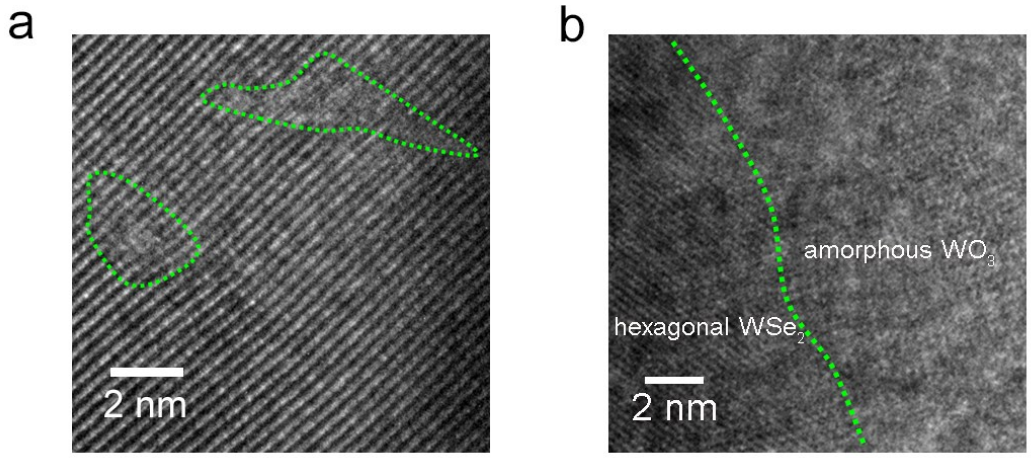

Figure S3. (a) HRTEM image of the WSe_2 region in the WO_3-WSe_2 heterostructure, showing very small oxidized amorphous regions (hightlighted by green dotted lines). (b) HRTEM image of the intermediate transition layer in the WO_3-WSe_2 heterostructure, showing amorphous WO_3 and hexagonal WSe_2. The interface between the hexagonal WSe_2 and amorphous WO_3 domains is hightlighted by the green dotted line.

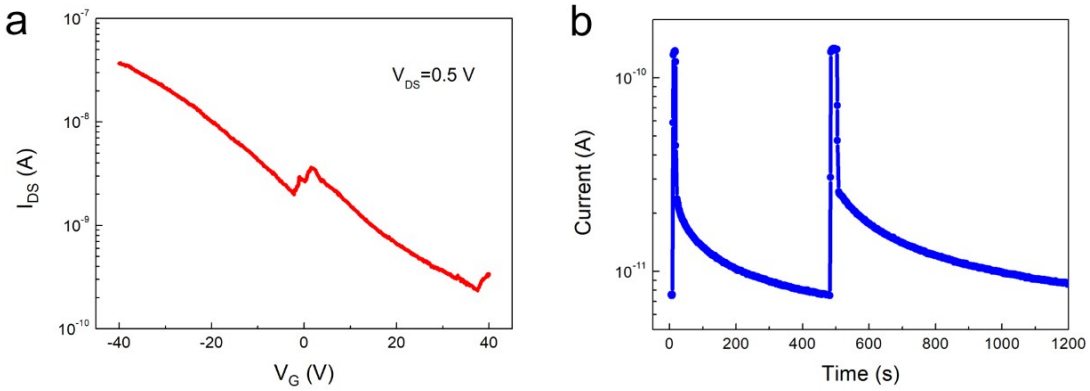

Figure S4. (a) Typical transfer curve of the Pd-WSe_2-WO_3-Pd device at V_{DS} = 0.5 V, which clearly shows *p*-type characteristics. (b) Typical photoresponse of the Pd-WO_3-WSe_2-Pd device at V_{DS} = 0.1 V. It exhibits a persistent photoconductivity (PPC) effect when turning off the light; the current decays to the initial state after the light is off.

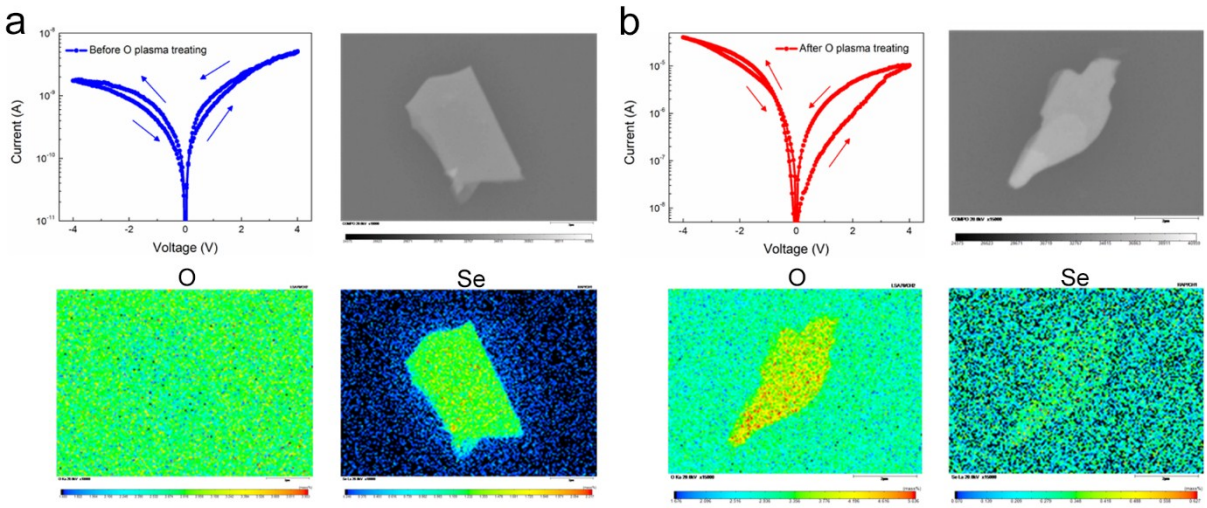

Figure S5. (a) *I-V* curve of the Pd-WSe_2-Pd device before the oxygen plasma treatment, and corresponding oxygen and selenium distributions as measured by EPMA. (b) *I-V* curve of the Pd-WSe_2-Pd device after the oxygen plasma treatment, and corresponding oxygen and selenium distributions as measured by EPMA. Before the oxygen plasma treatment, WSe_2 shows no oxidation and the Pd-WSe_2-Pd device exhibits no *I-V* hysteresis. After the oxygen plasma treatment, part of WSe_2 is oxidized into WO_{3-y}, consequently, the *I-V* hysteresis is observed in the Pd-WSe_2-Pd device.

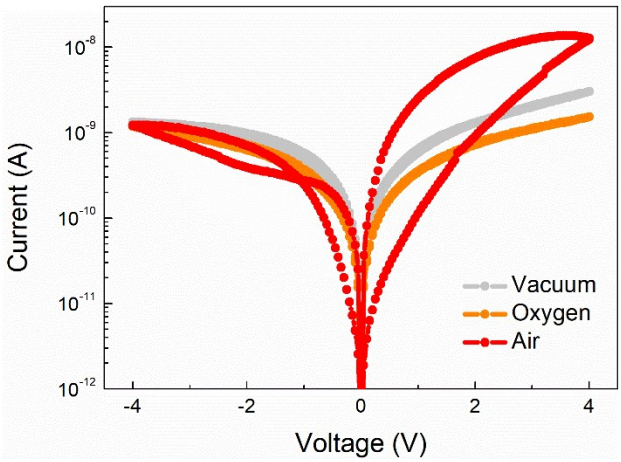

Figure S6. The *I-V* hysteresis as a function of ambient atmospheres, e.g. vacuum (10^{-6} Pa), pure oxygen and air. The *I-V* hysteresis disappears in vacuum and pure oxygen, but appears in air, demonstrating that the resistive switching is related to moisture in air.

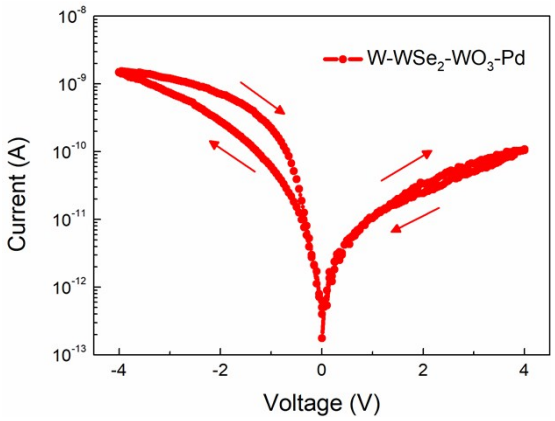

Figure S7. *I-V* characteristics of the W-WSe_2-WO_3-Pd device. It exhibits small *I*-V hysteresis because the hydrogen adsorption capacity of W is not as good as that of Pd.

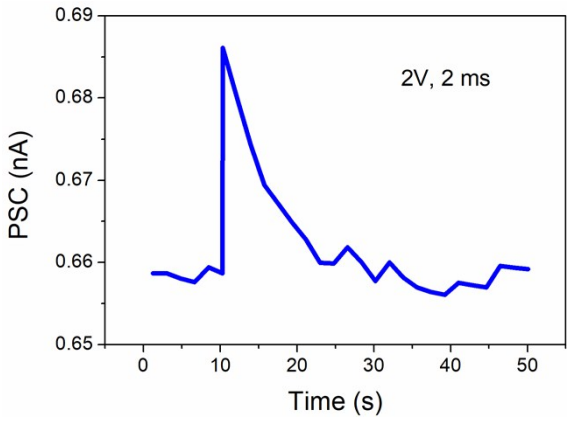

Figure S8. PSC triggered by electric pulse with amplitude of 2 V and width of 2 ms.

Energy consumption is calculated from the equation:
$E = I_{peak} \times V \times t$

Where I_{peak} is the maximum value of generated PSC, t is the pulse width, and V is the applied voltage. The energy consumption for a electric pulse (2 V, 2 ms) with I_{peak} of 0.685 nA is 2.7 pJ/spike. As the pulse width increases, the energy consumption increases.

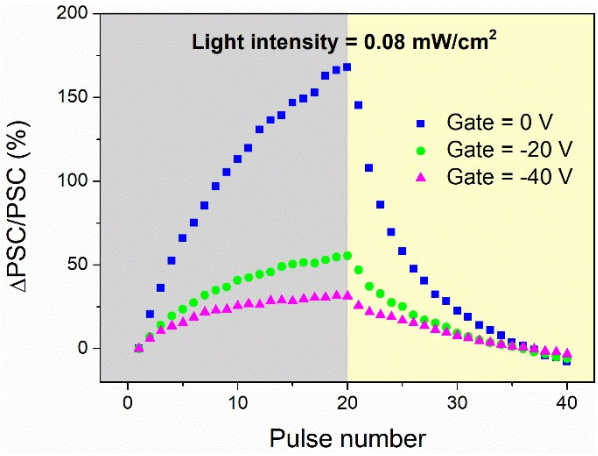

Figure S9. Synaptic characteristics controlled by simultaneously applying negative gate voltage and visible light.